Trapping-Assisted Sensing of Particles and Proteins Using On-Chip Optical Microcavities

Shiyun Lin and Kenneth B. Crozier*

School of Engineering and Applied Sciences, Harvard University, 33 Oxford Street, Cambridge, Massachusetts 02138, United States

ABSTRACT An improved ability to sense particles and biological molecules is crucial for continued progress in applications ranging from medical diagnostics to environmental monitoring to basic research. Impressive electronic and photonic devices have been developed to this end. However, several drawbacks exist. The sensing of molecules is almost exclusively performed *via* their binding to a functionalized device surface. This means that the devices are seldom reusable, that their functionalization needs to be decided before use, and that they face the diffusion bottleneck. The latter challenge also applies to particle detection using photonic devices. Here, we demonstrate particle sensing using optical forces to trap and align them on waveguide-coupled silicon microcavities. A second probe laser detects the trapped particles by measuring the microcavity resonance shift. We also apply this platform to quantitatively sense green fluorescent proteins by detecting the size distribution of clusters of antibody-coated particles bound by the proteins.

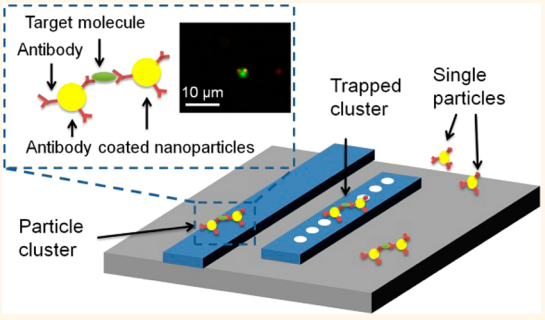

KEYWORDS: optical trapping · silicon photonics · resonator · protein sensing · particle sensing

Remarkable results have been recently obtained on the highly sensitive detection of analytes *via* the resonance shifts that result when they bind to the surfaces of optical microcavities.[1−6] Unlike traditional fluorescence-based biological sensing techniques such as enzyme-linked immunoassays (ELISA), microcavity-based sensors do not require complex chemical amplification or fluorescent labeling procedures. Microcavity-based sensors can possess ultrahigh sensitivity, a consequence of the enhanced light−matter interaction that arises from light being confined in the cavity for a long time.[7−11]

While impressive results have been obtained, microcavity sensing currently faces a number of obstacles. Typical microcavity sensing experiments involve the analyte binding to,[12] or being physically adsorbed by, the microcavity surface.[9−11] These methods introduce additional processes to attach and remove the analyte such as functionalizing the surface, immobilizing antibodies, and chemical or laser cleaning, thereby reducing sensing speed and increasing cost. Meanwhile, the resonance shift depends on the position of the analyte within the cavity mode,[10] which is especially problematic if the analyte consists of a discrete entity such as a nanoparticle. The lack of position control in current analyte loading methods makes the quantitative interpretation of experimental data therefore problematic.

In this paper, we demonstrate the real-time sensing of polystyrene particles using optical trapping and sensing. The large gradient of the evanescent field above the microcavity surface exerts forces on the particles that drag them to the surface.[8,13−15] Optical trapping provides a controllable means to load and release targeted particles.[14−18] This helps break the diffusion limit of the analyte. Compared to using physical adsorption to keep the particle in-place during sensing, this approach permits devices to be reused. The sensing reproducibility is also enhanced since the particles are self-aligned with the field maxima. In this paper, we trap and sense particles with a WGM microdonut cavity and with a nanobeam photonic crystal cavity. We furthermore demonstrate a new binding assay for protein sensing using our on-chip trapping-assisted sensing system.

* Address correspondence to kcrozier@seas.harvard.edu.

Received for review December 17, 2012 and accepted January 11, 2013.

Published online January 12, 2013
10.1021/nn305826j

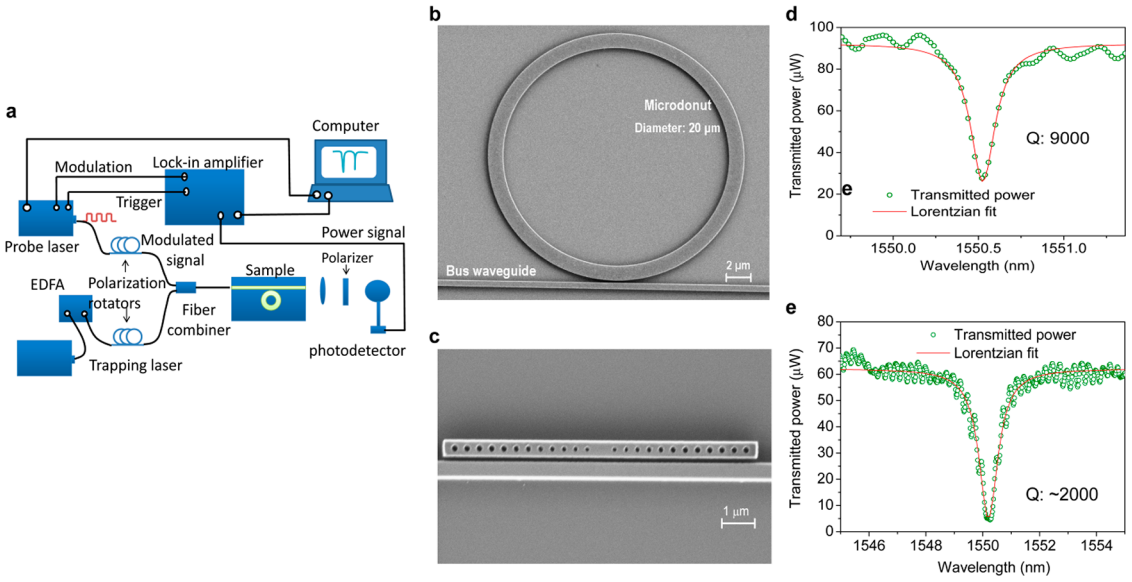

Figure 1. Measurement setup and fabricated devices. (a) Schematic diagram of measurement setup. (b,c) Scanning electron microscope (SEM) image of microdonut (b) and nanobeam photonic crystal cavity (d). (c,e) Transmission spectrum of the (c) microdonut and (e) nanobeam photonic crystal cavity. The microdonut has a *Q* of ~9000 for the transverse magnetic (TM) mode at the wavelength of 1550.5 nm, while a *Q* of ~2000 is measured for the transverse electric (TE) mode of photonic crystal cavity.

Instead of directly monitoring the resonance shift induced by molecules binding to a cavity, we measure the size distributions of clusters of antibody-coated particles bound by the molecules.

The experimental setup (Figure 1a) makes use of two tunable lasers, each operating around 1550 nm, to perform the trapping and sensing functions separately. As shown in the Supporting Information section S1 and the Supplementary Movie, a measurement interface is implemented using the software LabView (http://www.ni.com/labview), enabling viewing in real-time of the fluorescence microscopy image of the particles in the resonator vicinity, the resonator transmission spectrum, and the resonance wavelength as a function of time (measured since the start of the experiment). The trapping laser output is amplified by an erbium-doped fiber amplifier (EDFA) to achieve a high output power, passes through a polarization rotator, and is then input to a fiber combiner. The probe laser output passes through a polarization rotator, and is then also input to the fiber combiner. The fiber combiner output is focused into the photonic chip. The output of the photonic chip is focused onto a photodetector by a lens, with a polarizer used to select whether measurements are made on the TE or TM mode. The probe laser is modulated, with the modulation signal provided by a lock-in amplifier. This ensures that the probe laser component can be extracted from the photodetector signal using a lock-in amplifier. A home-built fluorescence microscope (not shown) is used to monitor fluorescent particles in the cavity vicinity.

RESULTS AND DISCUSSION

We first demonstrate trapping and sensing using a microdonut resonator (Figure 1b) with a *Q* of ~9000 (Figure 1d). The microdonut has an outer radius of 10 μm and width of 1 μm. A bus waveguide with a width of 500 nm is used to couple light into the microdonut. The gap between the microdonut and the bus waveguide is 200 nm. In Figure 2a, a measured shift in microdonut resonance wavelength is plotted as a function of the number of trapped particles. These have a diameter of 2 μm. The resonance wavelengths are determined by fitting the transmission spectra with a Lorentzian function, which provides a high sensing resolution even for a low *Q* cavity. The mean and standard deviation for each data point are obtained by averaging multiple scans ($\geq$6) performed under the same conditions. The error bars represent plus and minus 1 standard deviation from the mean. The results show a linear increase of resonance shift with the number of trapped particles, with the slope corresponding to a 30 pm resonance shift per particle. The peak shifts for particles with different diameters are also measured using the same approach (blue symbols and line, Figure 2b). One might expect the curve to show a superlinear behavior, being approximately proportional to the particle dipole moment,[19,20] which is in turn proportional to volume. The curve shows a sublinear behavior, however, but this can be explained by the fact that the fraction of each particle that overlaps with the closely confined evanescent field of the microcavity decreases with particle size. Using the system and microdonut resonators, we have trapped and sensed particles as small as 200 nm in diameter, which show a peak shift of 2.1 $\pm$ 0.4 pm.

We next investigate the use of a nanobeam photonic crystal cavity (Figure 1c) with a *Q* of ~2000 (Figure 1e)

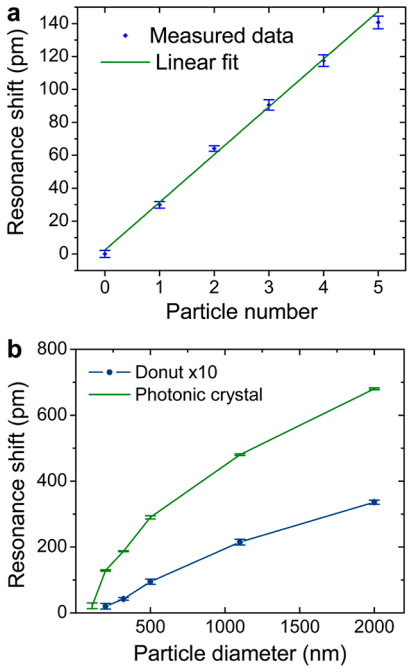

Figure 2. Particle counting and size sensing. (a) Resonance shift as a function of the number of trapped particles with a diameter of 2 μm. (b) Resonance shift as a function of particle diameter for the microdonut (blue) and photonic crystal cavity (green). The resonance shift values for the microdonut have been multiplied by 10 to facilitate comparison.

for trapping and sensing as a means for improving the sensitivity *via* its small mode volume. The photonic crystal cavity is fabricated by etching periodic holes into a Si channel waveguide. The holes are shifted outward to form a cavity in the center. The holes gradually increase in size from the center to reduce the scattering loss of the cavity mode and improve the *Q*. The cavity is coupled to a bus waveguide with a gap of 200 nm between them. Both the photonic crystal cavity and the bus waveguide have a width of 450 nm. The measured average resonance shifts as a function of particle diameter are shown as the green symbols and curve in Figure 2b. Particles as small as 110 nm diameter are trapped and detected, and show a peak shift of 21 ± 8 pm. The particle-induced resonance shifts for the photonic crystal cavity are larger than those of the microdonut, because of the cavity's smaller mode volume. The enhancement is 65-fold for the 200 nm particles (wavelength shift $\Delta\lambda$ increases from 2 to 130 pm), while 20-fold for the 2 μm particles ($\Delta\lambda$ from 34 to 680 pm). The enhancement is more profound for smaller particles, being closer to the factor of ~150 that one would expect from mode volume considerations alone. For both the photonic crystal and microdonut, the fraction of each particle that overlaps with the evanescent field decreases with increasing particle size. The increase in cavity mode perturbation is therefore smaller than one might anticipate from the particle size increase alone. The effect is more pronounced for the photonic crystal cavity than the microdonut, due to its larger in-plane confinement. It is for this reason that the resonance shift enhancement is more profound for smaller particles.

We now employ our trapping-assisted sensing method for the sensing of protein molecules. The detection of protein molecules lies at the heart of many medical diagnostic applications.[21] The traditional method by binding protein molecules to the functionalized surface of a high *Q* photonic resonator makes the device nonreusable, unless additional processes are introduced to regenerate the surface. Here, we demonstrate a new approach that overcomes this drawback by performing a binding assay with functionalized particles as carriers (Figure 3a). These polystyrene particles are coated with antibodies that specifically bind with the target protein molecules. The target molecules therefore cause the particles to aggregate into clusters. The particle clusters are trapped and detected by the microcavity. By measuring the resonance shifts of trapped particles, we can therefore detect molecules in solution without having them bind directly to the resonator.[22] Our approach enables determination of target molecule concentration from the measured histogram of resonance shifts. High concentration samples generate a larger proportion of clusters (and a smaller proportion of single particles) than low concentration samples. In addition to reusability, our approach enables a single device to detect different types of molecules, through the use of multiple bead types with different functionalizations. Lastly, because the molecules bind to beads in solution, rather than to a sensor on the wall of a microfluidic channel, our approach could help address the diffusion bottleneck problem present with low concentration samples.[1,23]

We choose green fluorescent protein (GFP) for our demonstration, which has a molecular weight of 27 kDa. Each GFP molecule possesses multiple active sites that can bind with its antibodies. A nanobeam photonic crystal cavity with the same design as Figure 1c is employed. As described further in the Supporting Information section S2, experiments involve adding antibody-coated particles to solutions containing GFP at different concentrations, then introducing the resultant mixture to the microfluidic chip containing the integrated photonic crystal cavities. For each sample, 80 particles or particle clusters are trapped, with the resonance shift determined for each. The results are shown as histograms in Figure 3b–e, with the trials sorted to place resonance shifts in ascending order. The results for a control sample containing no GFP are shown as Figure 3b. The resonance shifts are ~120 pm with a standard deviation of 7 pm. From the manufacturer's specifications, we estimate that particle size coefficient of variation contributes to the standard deviation by ~5 pm. Another factor that could contribute to the standard deviation is Brownian motion of the particles during the measurement interval.

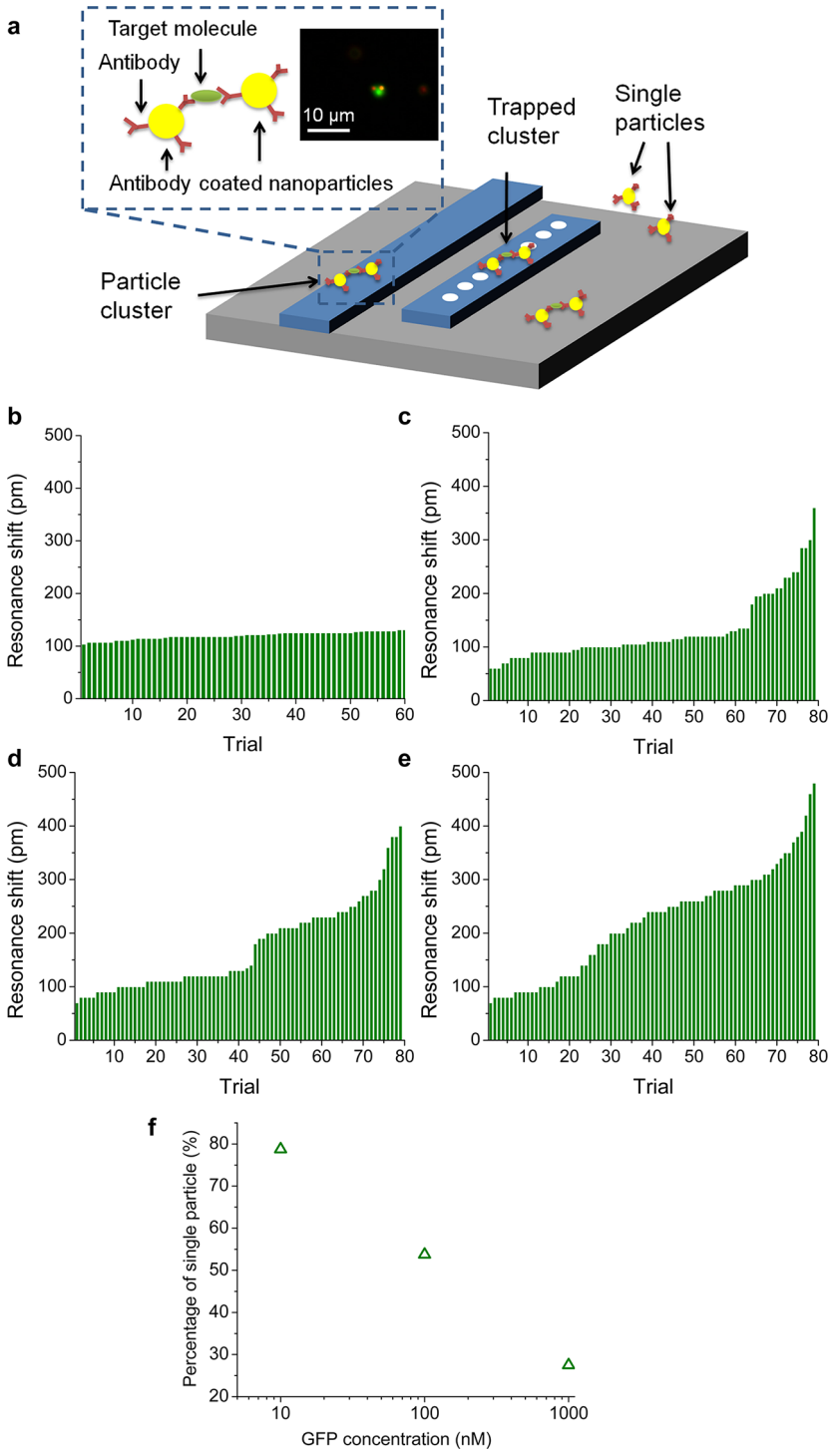

Figure 3. Binding assay for GFP sensing. (a) Schematic diagram of the binding assay. Inset: fluorescent microscopy image of a cluster with two particles bound by GFP. (b–e) Resonance wavelength shifts for samples (b) without GFP, and with GFP, at concentrations of (c) 10 nM, (d) 100 nM, and (e) 1 μM. (f) Percentage of trapping/sensing events that are single particles as a function of GFP concentration. Here, we assume the trials with a peak shift <141 pm (mean of the measured peak shift plus three times the standard deviation in Figure 3b) correspond to single particles.

The results of Figure 3b are consistent with the sample containing only single particles. We then perform experiments with a GFP concentration of 10 nM. The results (Figure 3b) demonstrate a marked step at trial 64. This indicates the trapping of particle clusters. The majority of the trapped objects (trials 1–63) are single particle with a resonance shift around 110 pm, with the remainder (trials 64–80) being clusters. In Figure 3d and e, we present results obtained for GFP concentrations of 100 nM and 1000 nM. It can be seen that the transition between single particles and clusters occurs at lower trial numbers, indicating a smaller fraction of

single particles for the higher concentration samples. This is because the probability of a particle encountering a GFP molecule, and therefore being able to bind with another particle, increases with GFP concentration. Further discussion on the probability distributions of measured resonance shifts for different GFP concentrations is provided in the Supporting Information section S3. Figure 3f plots the percentage of single particles as a function of GFP concentration. It can be seen that this method represents a quantitative tool for detecting the concentration of target molecules. In addition to depending on the details of the optical measurement technique, the sensing limit and dynamic range also depend on the properties of the binding process. Improving the binding efficiency would present a means for improving the sensing limit. Since the binding happens before the particles are trapped, the current approach is not suitable for applications requiring the monitoring of binding kinetics.

Sensing speed is an important parameter for cavity-based sensors, especially for quantitative analysis, where the number of detection events needs to be sufficiently large for meaningful results to be obtained. Our platform has several favorable attributes in this regard. The general approach to cavity sensing, in which molecules bind to the cavity surface, sometimes faces the drawback of long response time due to the properties of mass transport in microfluidic channels. In our approach, on the other hand, binding occurs outside the microfluidic channel. One could therefore use active mixing techniques to improve the binding efficiency still further. To improve the trapping rate, we use a combination of TE and TM modes, which effectively turns the long waveguide into a particle collector. The use of the waveguide as a particle collector is facilitated by the fact that it is patterned by lithography. There is therefore considerable flexibility in its design that is not present for cavities (e.g., microspheres or microtoroids) coupled to tapered optical fibers. The fact that the trapping and release of particles is controlled *via* polarization rather than laser power is also more favorable for achieving a high sensing speed. The particles trapped on the waveguide are continuously delivered to the cavity without interruption. This would not be the case if trapping were controlled by turning the laser on and off, because this would result in all trapped particles being released, including those on the waveguide. Lastly, we note that the concentration of the particles is chosen to enable a convenient trapping rate, with sufficient time between trapping events to perform sensing. In our experiments, the particle concentration (5.8×10^{15} particle/m^3) enables one measurement every ~30 s. The 80 trial measurements we perform therefore take ~40 min. The trapping efficiency is low due to the microfluidic channel being tall and the limited spatial extent of the optical force. Although the sensing results will not be affected, improving the trapping efficiency by reducing the channel height could reduce the analyte consumption.

CONCLUSION

In summary, we demonstrate the sensing of particles and proteins using a reusable integrated platform based on waveguide-coupled silicon microcavities (microdonuts or nanobeam photonic crystal cavities). The size and number of trapped particles are determined *via* monitoring microcavity resonance shifts in real time. The optical trapping-assisted sensing technique we introduce has the advantage of reusability. We apply our integrated trapping and sensing platform to detect proteins *via* antibody−antigen binding. In the presence of the target molecules, the antibody-coated particles form clusters that can be detected by our platform and quantitatively analyzed. This label-free, reusable, and reliable on-chip sensing system could be employed not only for the life sciences but also for a range of applications in nanotechnology and in environmental monitoring.

METHODS

Device Fabrication. The microdonut and nanobeam photonic crystal cavity are fabricated on a silicon-on-insulator (SOI) wafer. The SOI wafer has a 220 nm thick Si layer and a 3 μm thick buried oxide layer. The wafer is cleaved and coated with the negative-tone e-beam resist hydrogen silsesquioxane (HSQ). Electron beam lithography, development, and reactive ion etching are then performed. Smooth and vertical sidewalls are achieved using hydrogen bromide (HBr) gas as the Si etchant. The remaining HSQ is removed by dipping the chip into buffered oxide etch (BOE) solution. A microfluidic channel with a width of 200 μm and a height of 50 μm embedded in PDMS is bonded to the chip. For particle sensing experiments (Figure 2), fluorescent polystyrene particles in water are delivered to the microcavities through the microfluidic channel.

Protein Sample Preparation. To perform protein sensing, polystyrene particles with diameters of 320 nm are added to phosphate buffered saline (PBS) solution and mixed with the GFP antibody at room temperature for 2 h. The polystyrene particles are purchased from Invitrogen. The final concentration of the particles is 5.8×10^{15} particles/m^3. Solutions containing GFP at different concentrations are then added and mixed at 4 °C for 2 h. The mixed samples are kept at 4 °C for 48 h before the measurements. The time is not determined by the cluster formation but rather by the transportation of the samples from our collaborators.[24] Fluorescence microscopy (Figure 3a inset) confirms that aggregations of the antibody-coated particles are caused by the presence of the GFP molecules, though it does not of course yield the quantitative information of our microcavity method. Before measurements, the surfactant Tween 20 (0.1% v/v) is added to the solutions to prevent nonspecific binding between the particles and photonic sensor. In addition, before the measurements, casein blocking buffer is flowed through the microfluidic channel and incubated for 30 min to further prevent nonspecific binding.

Trapping and Sensing Measurement. The trapping and release of particles and particle clusters by the photonic crystal cavity is

controlled *via* varying the trapping laser polarization. The trapping laser polarization is first set so that 50% of the power is in the transverse electric (TE) mode, while the remaining 50% of the power is in the transverse magnetic (TM) mode. The TM mode exhibits enhanced electric fields on the top surface of the waveguide. The TM portion of the light therefore traps the particles onto the waveguide and propels them to the cavity. The TE mode couples to the photonic crystal cavity. The TE portion of the light, which generates high field enhancement in the cavity, therefore pulls particles from the bus waveguide to the cavity. The polarization of the probe laser is set to be the TE mode, to make it sensitive to resonance shifts of the photonic crystal cavity. The resonance wavelengths of the cavity before and after each trapping event are obtained by scanning the probe laser in a 5 nm bandwidth about the resonance wavelength at a rate of 5 nm/s. After each measurement, the trapped particle is returned to the waveguide by setting the trapping laser polarization to be completely the TM mode.

Conflict of Interest: The authors declare no competing financial interest.

Acknowledgment. This work was supported (in part) by the National Science Foundation (NSF) under Grant No. ECCS-0747560 (CAREER award) and (in part) by the Defense Advanced Research Projects Agency (DARPA) N/MEMS S&T Fundamentals program under Grant No. N66001-10-1-4008 issued by the Space and Naval Warfare Systems Center Pacific (SPAWAR). Fabrication work was carried out at the Harvard Center for Nanoscale Systems, which is supported by the NSF.

Supporting Information Available: Additional information on the trapping and sensing measurement in real time, protein sensing measurement procedure and probability distributions of measured resonance shifts for different GFP concentrations. This material is available free of charge *via* the Internet at http://pubs.acs.org.

REFERENCES AND NOTES

1. Squires, T. M.; Messinger, R. J.; Manalis, S. R. Making It Stick: Convection, Reaction and Diffusion in Surface-Based Biosensors. *Nat. Biotechnol.* **2008**, *26*, 417–426.
2. Sun, Y.; Fan, X. Optical Ring Resonators for Biochemical and Chemical Sensing. *Anal. Bioanal. Chem.* **2011**, *399*, 205–211.
3. Lee, M. R.; Fauchet, P. M. Nanoscale Microcavity Sensor for Single Particle Detection. *Opt. Lett.* **2007**, *32*, 3284–3286.
4. Dantham, V. R.; Holler, S.; Kolchenko, V.; Wan, Z.; Arnold, S. Taking Whispering Gallery-Mode Single Virus Detection and Sizing to the Limit. *Appl. Phys. Lett.* **2012**, *101*, 043704.
5. Ignatovich, F.; Novotny, L. Real-Time and Background-Free Detection of Nanoscale Particles. *Phys. Rev. Lett.* **2006**, *96*, 1–4.
6. Mandal, S.; Erickson, D. Nanoscale Optofluidic Sensor Arrays. *Opt. Express* **2008**, *16*, 1623–1631.
7. Vollmer, F.; Arnold, S. Whispering-Gallery-Mode Biosensing: Label-Free Detection down to Single Molecules. *Nat. Methods* **2008**, *5*, 591–596.
8. Arnold, S.; Keng, D.; Shopova, S. I.; Holler, S.; Zurawsky, W.; Vollmer, F. Whispering Gallery Mode Carousel—A Photonic Mechanism for Enhanced Nanoparticle Detection in Biosensing. *Opt. Express* **2009**, *17*, 6230–6238.
9. Zhu, J.; Ozdemir, S. K.; Xiao, Y.-F.; Li, L.; He, L.; Chen, D.-R.; Yang, L. On-Chip Single Nanoparticle Detection and Sizing by Mode Splitting in an Ultrahigh-Q Microresonator. *Nat. Photon.* **2009**, *4*, 46–49.
10. Lu, T.; Lee, H.; Chen, T.; Herchak, S.; Kim, J.-H.; Fraser, S. E.; Flagan, R. C.; Vahala, K. High Sensitivity Nanoparticle Detection Using Optical Microcavities. *Proc. Natl. Acad. Sci. U.S.A.* **2011**, *108*, 5976–5979.
11. He, L.; Ozdemir, S. K.; Zhu, J.; Kim, W.; Yang, L. Detecting Single Viruses and Nanoparticles Using Whispering Gallery Microlasers. *Nat. Nanotechnol.* **2011**, *6*, 428–432.
12. Xu, D.-X. D. X.; Vachon, M.; Densmore, A.; Ma, R.; Delâge, A.; Janz, S.; Lapointe, J.; Li, Y.; Lopinski, G.; Zhang, D.; *et al.* Label-Free Biosensor Array Based on Silicon-on-Insulator Ring Resonators Addressed Using a WDM Approach. *Opt. Lett.* **2010**, *35*, 2771–2773.
13. Lin, S.; Schonbrun, E.; Crozier, K. Optical Manipulation with Planar Silicon Microring Resonators. *Nano Lett.* **2010**, *10*, 2408–2411.
14. Chen, Y.-F.; Serey, X.; Sarkar, R.; Chen, P.; Erickson, D. Controlled Photonic Manipulation of Proteins and Other Nanomaterials. *Nano Lett.* **2012**, *12*, 1633–1637.
15. Cai, H.; Poon, A. W. Optical Manipulation of Microparticles Using Whispering-Gallery Modes in a Silicon Nitride Microdisk Resonator. *Opt. Lett.* **2011**, *36*, 4257–4259.
16. Lin, S.; Crozier, K. B. An Integrated Microparticle Sorting System Based on Near-Field Optical Forces and a Structural Perturbation. *Opt. Express* **2012**, *20*, 3367–3374.
17. Lin, S.; Crozier, K. B. Planar Silicon Microrings as Wavelength-Multiplexed Optical Traps for Storing and Sensing Particles. *Lab Chip* **2011**, *11*, 4047–4051.
18. Mandal, S.; Serey, X.; Erickson, D. Nanomanipulation Using Silicon Photonic Crystal Resonators. *Nano Lett.* **2010**, *10*, 99–104.
19. Arnold, S.; Khoshsima, M.; Teraoka, I.; Holler, S.; Vollmer, F. Shift of Whispering-Gallery Modes in Microspheres by Protein Adsorption. *Opt. Lett.* **2003**, *28*, 272–274.
20. Hu, J.; Lin, S.; Kimerling, L.; Crozier, K. Optical Trapping of Dielectric Nanoparticles in Resonant Cavities. *Phys. Rev. A* **2010**, *82*, 1–8.
21. Arruda, D. L.; Wilson, W. C.; Nguyen, C.; Yao, Q. W.; Caiazzo, R. J.; Talpasanu, I.; Dow, D. E.; Liu, B. C.-S. Microelectrical Sensors as Emerging Platforms for Protein Biomarker Detection in Point-of-Care Diagnostics. *Expert Rev. Mol. Diagn.* **2009**, *9*, 749–755.
22. Witzens, J.; Hochberg, M. Optical Detection of Target Molecule Induced Aggregation of Nanoparticles by Means of High-Q Resonators. *Opt. Express* **2011**, *19*, 7034–7061.
23. Sheehan, P. E.; Whitman, L. J. Detection Limits for Nanoscale Biosensors. *Nano Lett.* **2005**, *5*, 803–807.
24. The sample preparations were performed at Stanford University and then sent to Harvard. GFP antibody and GFP molecules are gifts from Dr. Yuan Cheng from the laboratory of Professor Hsueh, Stanford University.